Coherent superposition of photon- and phonon-assisted tunneling in coupled quantum dots

H. Qin,[1] A. W. Holleitner,[1] K. Eberl,[2] and R. H. Blick[1]

[1]*Center for NanoScience, Ludwig-Maximilians-Universität, Geschwister-Scholl-Platz 1, 80539 München, Germany*
[2]*Max-Planck-Institut für Festkörperforschung, Heisenbergstrasse 1, 70569 Stuttgart, Germany*
(Received 11 July 2001; published 12 November 2001)

We report on electron transport through an artificial molecule formed by two tunnel coupled quantum dots, which are laterally confined in a two-dimensional electron system of an $Al_xGa_{1-x}As/GaAs$ heterostructure. Coherent molecular states in the coupled dots are probed by photon-assisted tunneling (PAT). Above 10 GHz, we observe clear PAT as a result of the resonance between the microwave photons and the molecular states. Below 8 GHz, a pronounced superposition of phonon- and photon-assisted tunneling is observed. Coherent superposition of molecular states persists under excitation of acoustic phonons.

An artificial molecule is defined by coupling two quantum dots, leading to the formation of coherent electronic states in this molecule.[1–7] As a controllable two-level system, double dots are proposed for realizing a single quantum bit in solid-state systems.[8] One of the obstacles for such an application is the considerable dephasing induced by the semiconductor host materials. The investigation of dissipation processes in these nanostructures is thus of great importance. Operating such a double dot in the regime of weak coupling to the contacts ($\Gamma_{l,r} \rightarrow 0$) minimizes the dephasing of molecular states via the electron-electron interaction and it is then possible to study the interaction between confined molecular states and discrete phonon modes within the dots. Recently, Fujisawa *et al.*[9] found that at low temperatures vacuum fluctuations indeed result in pronounced transitions between energetically well-separated quantum states, generating discrete phonon modes. A theoretical treatment of this effect was then given by Brandes and Kramer.[10] However, the limitation of this experiment is that it can only be applied at large bias at which coherent molecular states can not be probed.

Here, we present transport measurements on a double-dot molecule coupled to both microwave photons *and* acoustic phonons. An external microwave source generates photons and piezoelectrically induces coherent acoustic phonons in phonon cavities formed by the Schottky gates. At near-zero bias, the formation of molecular states is revealed through single- and double-photon assisted tunneling (PAT). In addition, the combination of PAT with acoustic phonon-assisted tunneling is observed. We verify the persistence of coherent molecular states under phonon excitation.

As shown in Fig. 1, five pairs of Schottky gates are defined by electron-beam lithography and evaporation of gold on the surface of an $Al_xGa_{1-x}As/GaAs$ heterostructure. By applying proper negative voltages to these gates two quantum dots are formed in the two-dimensional electron system (2DES) located 90 nm below the surface. The left and right tunnel barriers determine the tunnel coupling of the double dot to the drain and source contact, respectively. The coupling conductance (G_c) between the dots is controlled by the central gate voltage (V_t) (see Fig. 1). At 4.2 K the carrier density of the 2DES is 1.7×10^{15} m^{-2} and the electron mobility is 80 m^2/Vs, yielding a mean free path of around 5 μm which is almost one order of magnitude larger than the dots'

effective diameters (~ 0.6 μm). The 2DES is cooled to a bath temperature of 140 mK in a ^{3}He/^{4}He dilution refrigerator. To couple microwave radiation to the quantum dots, we use a Hertzian wire-loop antenna about 1 cm above the dots, which is fed with an HP83711A microwave generator.[11]

The double dot is weakly coupled to the drain and source contacts, i.e., the tunneling rates of the outer left and right tunnel barriers are fixed around $\Gamma_l \approx \Gamma_r \sim 100$ MHz ($h\Gamma_l$, $h\Gamma_r \ll k_B T$, $\Delta\epsilon^*$, see below for the excited-state energy $\Delta\epsilon^*$). In the measurements, the drain-source bias V_{ds} is fixed at around -10 μV $\ll \Delta\epsilon^*/e$. When $V_{ds} < 0$ electrons tunnel through the double dot from drain to source. For characterization, charging diagrams are recorded by measuring the drain-source current while altering the left (V_{gl}) and right (V_{gr}) plunger gate voltages. We find the effective energy calibration factors $\alpha_{l/r}$ of 6×10^{-2} for both the left and right gate voltages and the addition energies are 351 μeV and 232 μeV for the left and right dot, respectively.[12] Both dots show excited states at $\Delta\epsilon^* \approx 120$ μeV. In Fig. 2(a) the charging diagram of the coupled dot is plotted in a linear grayscale representation in the weak coupling regime ($G_c \approx 0.08$ e^2/h). In linear transport, only two ground states par-
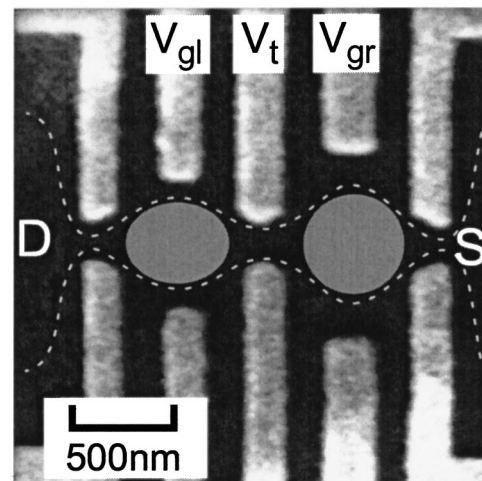

FIG. 1. Scanning electron microscope graph of this double dot. The dashed lines schematically show the edge of 2DEG. Two tunnel-coupled quantum dots are formed.
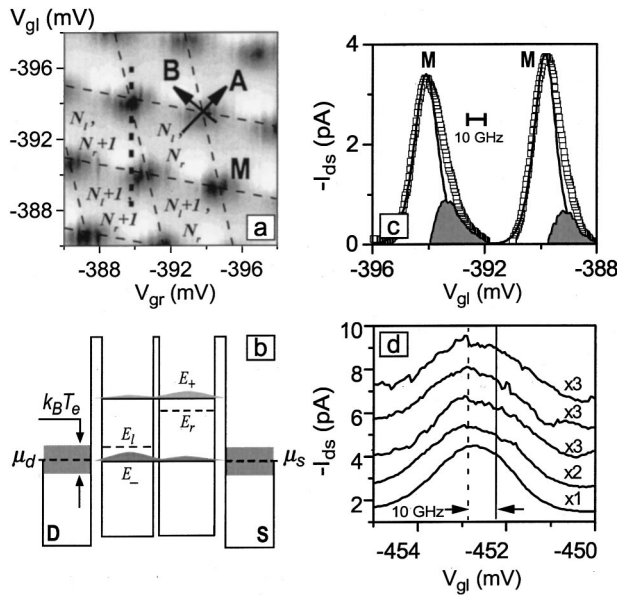
FIG. 2. (a) Charging diagram of drain-source current under weak tunnel coupling ($G_c \approx 0.08 \, e^2/h$) (linear scale, white: $I_{ds} \approx 0$ pA, black: $I_{ds} \geq -4$ pA). The charge configuration in the dots is denoted with (N_l, N_r). (b) The level diagram illustrates the resonant tunneling through the bonding molecular state. (c) A single trace extracted from (a) at a constant voltage (V_{gr}) marked by a vertical dashed line. (d) Temperature dependence of the peak asymmetry: At bath temperatures of 276, 320, 468, 564, and 634 mK for the curves from bottom to top, respectively.

ticipate, e.g., the ground state E_l in the left dot and E_r in the right dot, as schematically shown in Fig. 2(b).[13] The detuning between the two ground states is $E_{lr} = -(E_l - E_r)$. The finite tunnel coupling t between these two states induces a bonding (E_-) and an antibonding (E_+) molecular state, as shown in Fig. 2(b). The energetic offset between these states is $E_+ - E_- = \sqrt{E_{lr}^2 + 4t^2}$.[5,6] For weak tunnel coupling and nonzero detuning ($E_l \neq E_r$) it follows that a bonding electron is localized in one of the dots [as shown in Fig. 2(b)]. At zero detuning ($E_l = E_r$), the bonding electron tunnels back and forth between the dots at a Rabi frequency of $\Omega_R = 2t/h$. The discrete conductance peaks in Fig. 2(a) are main peaks (M) resulting from resonant tunneling through the molecular states with $E_{lr} = 0$.

Within the diamond-shaped regions [Fig. 2(a)] enclosed by dashed lines Coulomb blockade prevails and the number of electrons in the dots is well defined, corresponding to the charge configuration (N_l, N_r). In the direction marked by arrow **A** in Fig. 2(a), the detuning E_{lr} is kept constant, while the average of the ground-state energies $\bar{E} = (E_l + E_r)/2$ is increased relative to the chemical potentials (μ_d, μ_s) of the contacts. In direction of **B**, $\bar{E}$ is fixed but E_{lr} is varied. We find that the broadening in both directions is dominated by the temperature but not the intrinsic lifetime of the quantum levels: A signature of weak coupling to the contacts. The electron temperature in the contacts ($T_e \approx 170$ mK) is obtained simply by measuring the full width at half maximum (FWHM) of the conductance peak of a single quantum dot.[14–16] In direction of **B**, the FWHM of about 70 μeV is
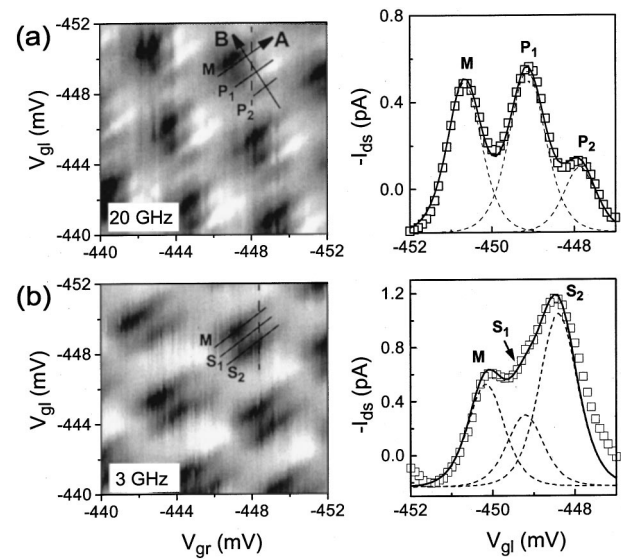

FIG. 3. Charging diagrams of the weakly coupled double dot ($G_c \approx 0.08 e^2/h$) under microwave radiation at (a) 20 GHz and (b) 3 GHz (white: $I_{ds} \approx 0$ pA, black: $I_{ds} \geq -4$ pA). The corresponding single traces extracted from the linear grayscale plot at a constant V_{gr} (marked by dashed lines in the charging diagrams) show the details.

lower than that in direction of **A** (~ 100 μeV).[17] The level diagram shown in Fig. 2(b) takes into account the temperature broadening in the contacts.

The charging diagram shown in Fig. 2(a) exhibits electron transport by thermally induced phonons. To clarify this, a typical single trace extracted from the diagram is shown in Fig. 2(c). On the left side of the peak, where $E_l > E_r$, the data is well approximated by $\cosh^{-2}(E_{lr}/2k_B T_e)$. This implies that transport at the center of the peak is dominated by resonant tunneling through a molecular state with $E_{lr} = 0$ [see the solid line in Fig. 2(c)]. However, on the right side where $E_l < E_r$, an additional contribution to the tunneling current is found, which has a maximum [see the dark region in Fig. 2(c)] about 10 GHz away from the main peak. By increasing the bath temperature, we find the position of this maximum to shift slightly to the right side, as shown in Fig. 2(d). We can exclude both electronic excitations from the drain and source contacts ($|eV_{ds}| \approx 10$ μeV $< h \cdot 3$ GHz) and intrinsic excitations in the dots ($\Delta \epsilon^* \approx 120$ μeV $\approx h \cdot 30$ GHz) inducing this additional tunneling. Furthermore, tunneling through the bonding or antibonding molecular state with $E_{lr} \neq 0$ is strongly suppressed in this weak coupling regime ($E_+ - E_- \cong E_{lr}$). Hence, we can attribute this additional off-resonant tunnel current to be induced by a background of acoustic phonons.

Application of microwave radiation allows us to perform spectroscopy on single quantum states by measuring the direct photoresponse.[4–6] Figure 3(a) shows a charging diagram of the weakly coupled dot ($G_c \approx 0.08 e^2/h$) under microwave radiation at a frequency of $f = 20$ GHz. As seen in the right panel of Fig. 3(a), in addition to the main resonant tunneling peak (M) two side-peaks (P_1, P_2) appear. Tunneling at the side-peaks is enabled by the resonance between the micro-
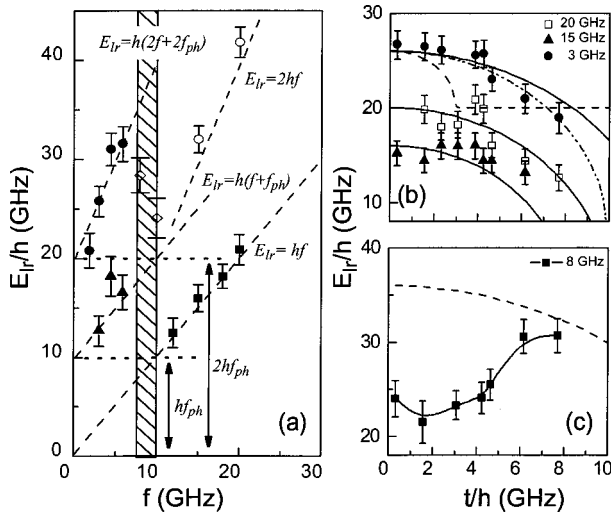
FIG. 4. (a) The detuning at side-peaks P_1, P_2, S_1 and S_2 versus microwave frequency in the weak tunnel coupling regime ($G_c \approx 0.08\ e^2/h$). $f > 10$ GHz: Solid squares and open circles are for side-peaks P_1 and P_2, respectively. $f < 8$ GHz: Solid triangles and solid circles stand for side-peaks S_1 and S_2, respectively. In the hatched region (8–10 GHz), the open diamonds correspond to side-peaks S_2. (b) The coupling dependence of the detuning at side-peaks P_1 and S_2 at 3, 15, and 20 GHz. For 15 and 20 GHz, the solid lines correspond to Eq. (3). For 3 GHz, the dashed line is from Eq. (4), the dashed/dotted line is fitted with Eq. (5), and the solid line is based on Eq. (6). (c) At 8 GHz, the dashed curve is calculated from Eq. (6).

wave photons and the energy difference between the molecular states: $E_+ - E_- = nhf \cong E_{lr}$, $n = 1, 2, \dots$. Side-peaks P_1 and P_2 correspond to one-photon ($n = 1$) and two-photon ($n = 2$) absorption processes, respectively. In the right panel of Fig. 3(a), the solid line is an approximation including three peaks according to $\cosh^{-2}((E_{lr} - nhf)/2k_B T_e)$, with $n = 0$ for the main peak (M) and $n = 1, 2$ for P_1 and P_2. For frequencies above 10 GHz this can be clearly seen in Fig. 4(a) where filled squares (open circles) denote the distance of the P_1 (P_2) side-peaks.

Below 10 GHz, two side-peaks (S_1, S_2) are resolved from the charging diagrams. In Fig. 3(b), the charging diagram at 3 GHz is shown. The single trace in the right panel is approximated by three $\cosh^{-2}(E_{lr}/2k_B T_e)$-shaped peaks. The peak S_1 is masked between the main peak M and the side-peak S_2. The existence of S_1 is confirmed under microwave radiation at 3, 4.5, and 5.9 GHz. For the detuning at side-peaks S_1 and S_2, we find the following relations:

$$E_{lr}^{S_1} \approx h(f + f_0), \tag{1}$$

$$E_{lr}^{S_2} \approx 2h(f + f_0), \tag{2}$$

with a constant offset of $f_0 \approx 10$ GHz, as shown in Fig. 4(a). The slopes of the traces correspond to absorption of one and two photons. The offset, however, indicates that transport through the dots involves not only pure photon absorption processes, but also another absorption process of hf_0 or $2hf_0$.

We attribute this offset energy quanta in Eqs. (1) and (2) to acoustic phonons at $f_{ph} \approx f_0 \approx 10$ GHz. As discussed above, we observe thermally induced acoustic phonons already without microwave radiation, as shown in Fig. 2(c) and 2(d). Additionally, the Schottky gates on the heterostructure surface not only define the quantum dots, but also form phonon cavities since $Al_xGa_{1-x}As/GaAs$ is a piezoelectric material.[9] Electrons in the quantum dots confined only 90 nm below the heterostructure surface thus mainly couple to local phonon modes within the cavities. Furthermore, the applied microwave field enhances via piezoelectrical coupling the interaction of electrons and phonons localized within the cavities. Experimentally, strong photon side-peaks shifted by $f_{ph} \approx 10$ GHz are observed in the microwave frequency range from 1 to 6 GHz. This phonon frequency is determined by the size of the cavities. Assuming a sound velocity of about 4500 m/s in bulk GaAs crystals and a phonon frequency of 10 GHz, we find a wavelength of 450 nm. This roughly agrees with the dots' diameters as shown in Fig. 1. Moreover, this piezoelectrical resonator formed by Schottky gates possesses a large bandwidth, due to the limited number of gates in comparison to conventional interdigitated transducers.[18] Hence, exciting this transducer off resonance will also generate phonons at 10 GHz as verified experimentally. Most importantly, confined phonons generated by the microwave field are naturally coherent with the microwave photons. Finally, no significant heating by microwaves is observed. Indeed, the much stronger side-peaks under radiation [see Fig. 3] compared to the weak shoulder without radiation [see Fig. 2(c)] confirm that the confined phonon mode at $f_{ph} \approx 10$ GHz in the cavities is enhanced.

The central question now is to verify the coherent superposition of molecular states by microwave photons under the excitation of acoustic phonons. For this purpose, charging diagrams under radiation are measured upon increasing the tunnel coupling. From these diagrams, the coupling dependence of the detuning of two quantum states, at which the two molecular states are in resonance with microwave photons, are obtained. As shown in Fig. 4(b), we find that at 15 and 20 GHz the detuning at side-peak P_1 follows the well-known relation

$$E_{lr} = \sqrt{(hf)^2 - 4t^2}, \tag{3}$$

where it is simply assumed that $t \propto G_c$. Equation (3) is a signature of a coherently coupled two-level system as studied before.[4–6]

Commonly, one expects no coherent superposition of the molecular states by single-photon resonance below $f = 8$ GHz, since the thermal fluctuations are comparable to the photon energy. Nevertheless, the coupling dependence obtained at 3 GHz turns out to be quite similar to those at 15 and 20 GHz: Due to the participation of both photons and phonons the detuning at resonance is larger than without phonons. Furthermore, the detuning at resonance decreases as the tunnel coupling is enhanced [see Fig. 4(b)], behaving like Eq. (3). Considering the dynamics of electron transport at 3 GHz, the processes of phonon and photon absorption between the dots can be coherent as well as sequential. The

first sequential process to be considered is the following: Phonon absorption occurs within the single dots exciting an electron into an intermediate state, while photon absorption couples the dots, i.e.,

$$E_{lr} = \sqrt{(2hf)^2 - 4t^2} + 2hf_{ph},\qquad(4)$$

being depicted by the dashed curve in Fig. 4(b) for the side-peaks S_2,[19] which is obviously not observed. The other sequential process is given by the absorption of photons in the dots but the dots are coupled by phonon absorption. The corresponding coupling dependence follows

$$E_{lr} = \sqrt{(2hf_{ph})^2 - 4t^2} + 2hf,\qquad(5)$$

depicted by the dashed/dotted trace in Fig. 4(b), which is in reasonable agreement with the experimental data. On the other hand, assuming coherent photon and phonon generation by the microwave source, an electron tunneling coherently between the dots can absorb both photons and phonons. The coupling dependence is then written as

$$E_{lr} = \sqrt{[2hf + 2hf_{ph}]^2 - 4t^2},\qquad(6)$$

illustrated by the solid curve for $f = 3$ GHz in Fig. 4(b). Within the error bars also this process can be assumed. The coherent absorption of both two-phonons and two-photons by an electron can be viewed as a two-quanta absorption process, while the sequential absorption is a four-quanta process, which has an even smaller probability. The observed strong side-peaks S_1 and S_2 at 3, 4.5, and 5.9 GHz imply the coherent absorption of both microwave photons and acoustic phonons. This is supported by the fact that microwave photons are excited coherently with acoustic phonons via the Schottky gates. The superimposed molecular states in the double dot are not demolished by absorbing acoustic phonons, which is in agreement with the theoretical prediction by Smirnov *et al.*[20] Finally, the hatched area in Fig. 4(a), marks a transition region between 8 and 10 GHz. An increase of the coupling at 8 GHz enhances the detuning at resonance [see Fig. 4(c)], i.e., in this transition region no simple superposition of photon and phonon modes exists.

To summarize we connect two quantum dots of medium size and probe the coherent coupling of the discrete states under near zero bias by using microwave spectroscopy. The applied radiation coherently excites photons and acoustic phonons via the Schottky gates. Apart from conventional photon-assisted tunneling observed above 10 GHz, we find a coherent superposition of photon- and phonon-assisted tunneling below 8 GHz. We conclude that molecular states in the double dot persist under the excitation of acoustic phonons.

[1] L. P. Kouwenhoven *et al.*, in *Mesoscopic Electron Transport, Proceedings of a NATO Advanced Study Institute*, edited by L. L. Sohn, L. P. Kouwenhoven and G. Schön (Kluwer, Dordrecht, 1997), Ser. E, Vol. 345.

[2] C. Livermore, C.H. Crouch, R.M. Westervelt, K.L. Campman, and A.C. Gossard, Science **274**, 1332 (1996).

[3] R.H. Blick, D. Pfannkuche, R.J. Haug, K.v. Klitzing, and K. Eberl, Phys. Rev. Lett. **80**, 4032 (1998); R.H. Blick, D.W. van der Weide, R.J. Haug, and K. Eberl, *ibid.* **81**, 689 (1998).

[4] T.H. Oosterkamp, T. Fujisawa, W.G. van der Wiel, K. Ishibashi, R.V. Hijman, S. Tarucha, and L.P. Kouwenhoven, Nature (London) **395**, 873 (1998).

[5] C.A. Stafford and N.S. Wingreen, Phys. Rev. Lett. **76**, 1916 (1996).

[6] T.H. Stoof and Yu.V. Nazarov, Phys. Rev. B **53**, 1050 (1996).

[7] A. W. Holleitner, C. R. Decker, K. Eberl, and R. H. Blick, cond-mat/0001144.

[8] D. Loss and D.P. DiVincenzo, Phys. Rev. A **57**, 120 (1998).

[9] T. Fujisawa, T.H. Oosterkamp, W.G. van der Wiel, B.W. Broer, R. Aguado, S. Tarucha, and L.P. Kouwenhoven, Science **282**, 932 (1998); T. Fujisawa, W.G. van der Wiel, and L.P. Kouwenhoven, Physica E (Amsterdam) **7**, 413 (2000).

[10] T. Brandes and B. Kramer, Phys. Rev. Lett. **83**, 3021 (1999).

[11] H. Qin, F. Simmel, R.H. Blick, J.P. Kotthaus, W. Wegscheider, and M. Bichler, Phys. Rev. B **63**, 035320 (2001).

[12] The factors α_l and α_r are defined as $\alpha_{l/r} = \delta E_{lr}/e\,\delta V_{gl/gr}$, where $E_{lr} = -(E_l - E_r)$ represents the detuning between two quantum states in the left and right dot. The addition energy is defined as $E_\Sigma = e^2/C_\Sigma + \delta\epsilon$, where C_Σ and $\delta\epsilon$ represent the total capacitance and the level spacing for the single dots.

[13] For simplicity, we adopt a rather simple picture here. In fact, $E_{l/r}$ represents the chemical potential of the left/right dot associated with the ground-state transition $N_{l/r} + 1 \leftrightarrow N_{l/r}$ when it is aligned with the chemical potential of the drain/source contact.

[14] C.W.J. Beenakker, Phys. Rev. B **44**, 1646 (1991).

[15] E.B. Foxman, P.L. McEuen, U. Meirav, N.S. Wingreen, Y. Meir, P.A. Belk, N.R. Belk, M.A. Kastner, and S.J. Wind, Phys. Rev. B **47**, 10 020 (1993).

[16] D. Goldhaber-Gordon, J. Göres, M.A. Kastner, H. Shtrikman, D. Mahalu, and U. Meirav, Phys. Rev. Lett. **81**, 5225 (1998).

[17] The tunnel splitting in direction **A** can be neglected when two dots are weakly coupled. The splitting observed results from the electrostatic coupling of the two dots, which is proportional to the interdot capacitance.

[18] A. Wixforth, J. Scriba, M. Wassermeier, J.P. Kotthaus, G. Weimann, and W. Schlapp, Phys. Rev. B **40**, 7874 (1989); A. Wixforth (private communication).

[19] Here we only show the coupling dependence of the detuning at side-peak S_2 since it has smaller error than that of side-peak S_1.

[20] A.Yu. Smirnov, N.J.M. Horing, and L.G. Mourokh, Appl. Phys. Lett. **77**, 2578 (2000).